

## STEEL BEAM–COLUMN JOINT WITH DISCONTINUOUS VERTICAL REINFORCING BARS

Ju-Yun HU, Won-Kee HONG

*Department of Architectural Engineering, Faculty of Architectural Engineering,  
Kyung Hee University, 446-701 Yongin, Korea*

Received 10 Nov 2015; accepted 08 Jan 2016

**Abstract.** The authors have previously proposed steel beam–column connections for precast concrete frames. The steel–concrete composite frames combined the advantages of the fast assembly of steel and the low cost of concrete structures. However, when not enough space is available at column–beam joints, steel sections from beams cannot be connected with column brackets. To address this issue, this paper explores the strategy of disconnecting some vertical reinforcing bars at the joints by connecting vertical steel reinforcements to steel plates placed above and below column steels, to provide a load transfer path. Loads from re-bars are transferred to steel plates, column steels, and back to steel plates and re-bars below the column steels. This strategy provided space for beam–column joints of composite frames. Extensive experiments were performed to verify load transfer from re-bars to steel plates above joints and from the steel plates to re-bars below the joint. The flexural load-bearing capacity of a column with a total of 24 vertical re-bars was compared to that of columns with discontinuous re-bars at the joints; the number of discontinuous re-bars at the joint used in the column specimens tested was 0 (0.0%), 4 (16.7%), 12 (50.0%), and 20 (83.3%).

**Keywords:** beam–column connections, column brackets, composite frames, load transfer, continuous and discontinuous re-bars, reductions in moment resisting capacity, conflicting joint details.

### Introduction

Due to their high ductility and energy dissipation, composite structures are currently widely adopted in high-rise buildings as lateral-force-resisting systems. In order to understand their behaviour in typical applications and their benefits over pure steel or concrete systems, extensive and careful research needs to be conducted regarding the behaviour of composite beam–column joints. This paper introduces a new beam–column joint connection in which some vertical reinforcing bars are disconnected at joints by connecting vertical steel reinforcements to steel plates placed above and below column steels to provide a load transfer path. In cases where there are conflicting structural details between vertical column re-bars and column brackets during the construction of steel–concrete composite frames, spaces are provided to place these structural components where they should be. This conflict, illustrated in Figure 1, can be resolved by disconnecting vertical re-bars, with the trade-off of some reductions in moment resistance. However, this reduction in strength can be minimized or counterbalanced by introducing high-strength steel plate at the joints. In the present work, new beam–column joint connections for steel–concrete composite frames were designed, with

structural details based on extensive experimental and analytical investigations.

The main studies related to composite structures have had the aim of understanding the behaviors of beam–column joints subjected to various types of loads. Liew *et al.* (2000) conducted research on six full-scale composite column joints; in their experiment, the steelwork connection consisted of a flush end-plate welded to the beam end. They suggested a simple spring model for the slab combined with a simple spring model for the steel joint, and showed that this combined model predicted the moment capacity of composite joints well, although it seemed to over predict rotational stiffness. Similarly, four full-scale flush end-plate semi-rigid beam–column joints were fabricated and tested by Ataei *et al.* (2015). Recently, Hu *et al.* (2014) analytically investigated pre-fabricated steel beam–column connections under cyclic loading to further investigate their seismic performance. There have also been reports dealing with the seismic performance of beam–column joints (Zhang *et al.* 2012; Kumar, Smitha 2013; Qin *et al.* 2014a; Liew *et al.* 2004). Although beam–column connections are designed to fully transfer moment through the interconnected members,

This article has been corrected since first published. Please see the statement of correct (<https://doi.org/10.3846/13923730.2017.1328020>).

Corresponding author: Won-Kee Hong  
E-mail: [hongwk@khu.ac.kr](mailto:hongwk@khu.ac.kr)

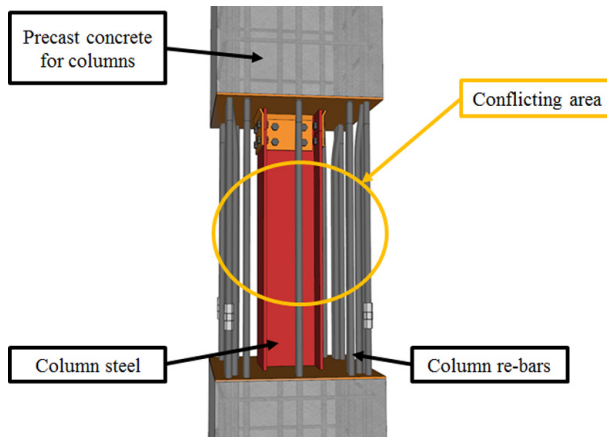


Fig. 1(a). Conflicting joint details between vertical column re-bars and column bracket

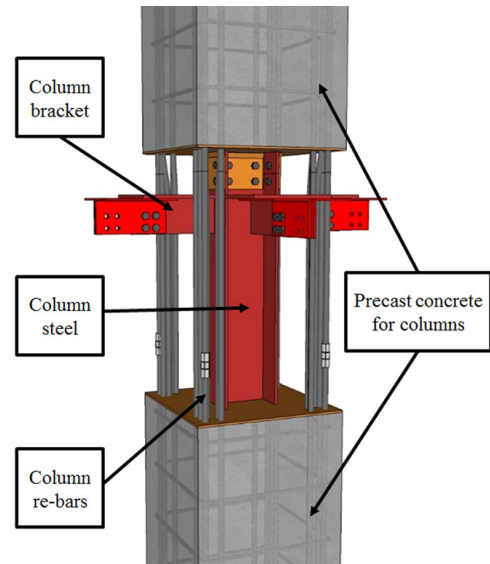


Fig. 1(b). Column brackets attached to column steel

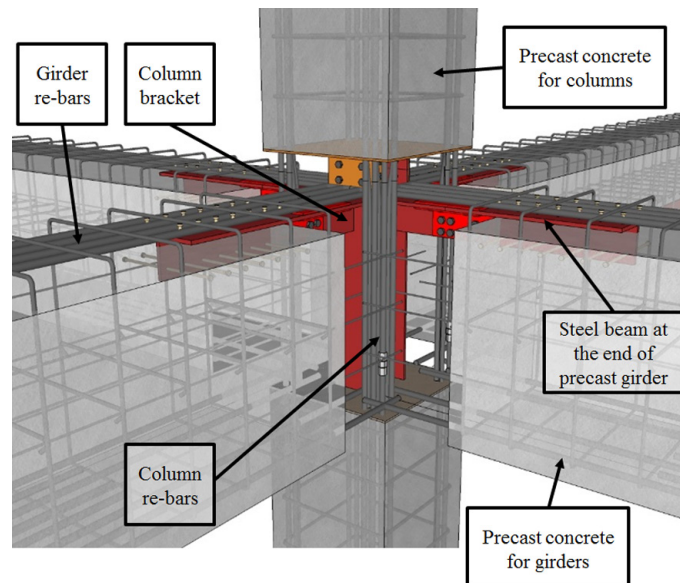


Fig. 1(c). Girders connected to column brackets

Fig. 1. Conflicting joint details between vertical column re-bars and column bracket

some of them behave semi-rigidly. Some studies (Simões da Silva *et al.* 2001; Fang *et al.* 1999) have been conducted with the aim of improving the structural performance of joint connections in composite steel–concrete composite structures.

Bjorhovde *et al.* (1990) developed a scheme whereby connections can be classified in terms of strength, stiffness, and ductility, using tests and theoretical data; they presented a new arrangement of connection types to fit into an existing database. In addition, theoretical design equations and design guidelines have also been proposed (Qin *et al.* 2014b, 2014c; Sheikh *et al.* 1989; Deierlein *et al.* 1989), including demonstrations that the proposed theoretical equations provide good correlations

between predicted and experimentally measured strength. Hajjar (2002) summarized recent research on a number of composite lateral-force-resisting structures including braced and unbraced frames. Later, Salvatore *et al.* (2005) conducted parametric analyses focusing on the influence of a composite slab's strength upon joint performance. Kataoka and El Debs (2014) conducted another parametric study of composite beam–column connections using 3D finite element modelling; their parametric analysis of beam–column joints for composite structures included investigations of bolt diameter, stud spacing, and slab reinforcement ratio. Limited number of studies has been carried out over past years to assess the effect of composite joints on the behaviour of building frames. It

is clear that the process of establishing a standardized joint design for steel-concrete frames has been slowed because of a large number of parameters affecting their behaviour. Importantly, steel-concrete joints introduced in previous studies require fire proofs for steel members since steel beams are not encased by concrete. The novel beam-column joint proposed in this study, provides not only an advantage of constructability and assembly time of steel frame but also it doesn't require fireproofs for steel sections since steel members are encased by concrete. Steel joint for the precast column–beam connection was rarely adapted to provide moment connections until it was suggested in this study. Concrete must be cast to provide moment connection for the conventional precast column–beam joints. It is noted that the delayed construction schedule compared with the steel joint introduced in this study is inevitable.

### 1. Problem statement

Composite beams which were used for similar practice in Europe and U.S.A. were shown in Figure 2. In these applications, floor slabs were installed on the bottom flange of beams to reduce beam depth, however, requiring fire proofs for steel members since steel beams were not encased by concrete. The column-beam connections in these frames were mainly based on steel joint, differing from the one suggested in this study.

In this paper, the use of composite frames with steel beams at the end illustrated in Figure 2 was suggested to contribute to the adaptation of the constructability of steel works, eliminating fire proofs. The joint of precast concrete columns and beams were assembled by steel members, offering efficient structural strength based on steel-concrete composite actions to resist moment at both ends while providing joint connections with column steels to introduce an advantage of similar constructability and assembly time of steel frame for precast concrete frame. The interaction between the two materials with integrating pre-cast concrete with steel components presents advantages in terms of reduced structural steel tonnage, shortened construction schedules, and eliminated fire proofs. The precast composite beam has also shown the outstanding structural efficiencies to reduce beam depth as published in the previous works of authors (Hong *et al.* 2008a, 2008b, 2015).

### 2. Method of experimental investigation

Figure 3(a) illustrates a test specimen including 4 continuous vertical reinforcing bars and 20 vertical re-bars that were cut off by connecting them to steel plates by means of bolts, above and below the column steel. Specimens were designed to verify the load path along vertical re-bars. The steel plates above the column steel picked up loads from the re-bars (Fig. 3(b)). The loads moved down to the steel plate through the column steel and further down to the lower steel plate. Finally, column loads were picked up by the vertical re-bars again.

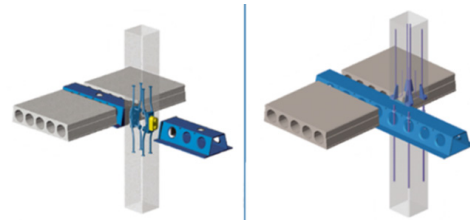


Fig. 2(a). Delta beam in Europe

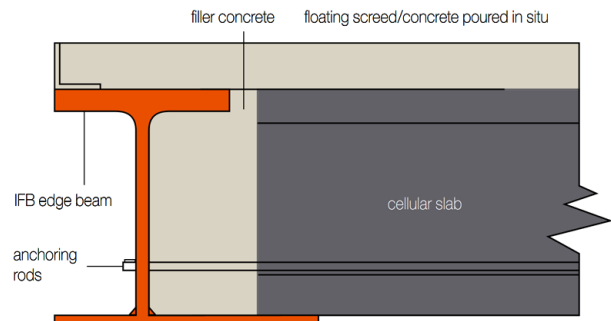


Fig. 2(b). Slim floor beam in Europe

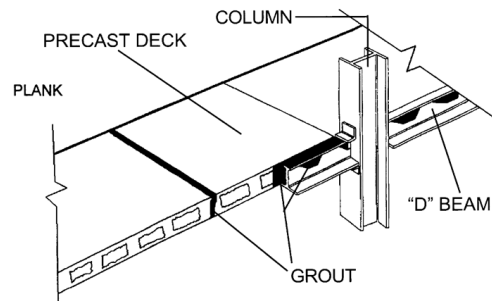


Fig. 2(c). Flex beam in USA

Fig. 2. Composite beams offering floor depth reduction

The load capacity lost during the path was measured experimentally, and these measurements were used to develop recommendations for joint connection design. The flexural load-bearing capacity of a control column with a total of 24 vertical re-bars was compared to that of columns in which there were 4 (16.7%), 12 (50.0%), and 20 (83.3%) discontinuous re-bars. Figure 3(c) shows the structural details of the bolted connection between re-bars and plate. Figure 3(d) indicates gauge arrangement with gauge numbers attached to concrete, re-bars and steel sections.

Figure 4(a) shows the test setup for the specimens with details for vertical reinforcing bars bolted to plates. The distance from the base to the centre of loading was set as 1.5 m. The test was loaded by the displacement control method with the loading protocol illustrated in Figure 4(b). A 1000 kN actuator with a stroke of 300 mm was used to exert cyclic loading onto the specimens. LVDTs were installed vertically and horizontally as shown in Figure 4(a) to accurately measure deformation in the specimens. Figure 5 shows the strain gauges

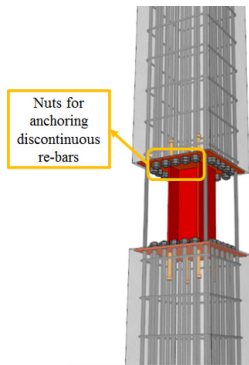


Fig. 3(a). Test column specimen with discontinuous re-bars (Specimen #4; 20 re-bars cut off)

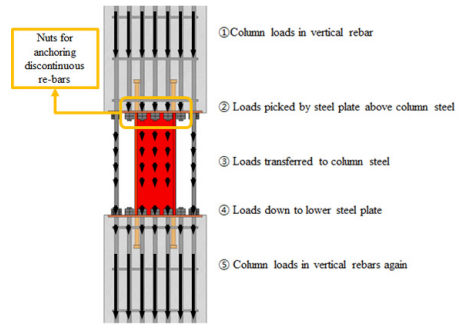


Fig. 3(b). Load path along the column (Specimen #4; 20 re-bars cut off)



Fig. 3(c). Discontinuous re-bars connected to steel plates by bolts (Specimen #3; 12 re-bars cut off)

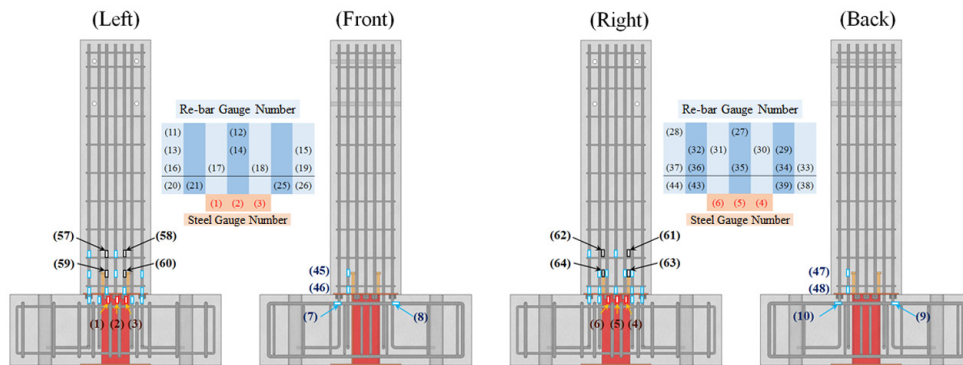


Fig. 3(d). Strain gauge plan (Specimen #3; 12 re-bars cut off)

Fig. 3. Design and manufacture of test specimen (Specimen #3, 4)

used to measure strains of re-bars at various locations. Figure 6 depicts the deformed specimen under the application of load.

### 2.1. Specimen manufacture

Specimens were made of foundations 1500 mm × 1500 mm wide and 500 mm tall, and columns 1800 mm long that were reinforced with 24 re-bars of diameter 22 mm (Fig. 7). The yield strength of re-bars was 500 MPa. The 500 mm × 500 mm columns were supported by foundations with steel sections installed at the joint,

as depicted in the figure. The steel sections were 200 mm (B) × 200 mm (H) × 8 mm (tw) × 12 mm (tf) and had the yield strength of 325 MPa. The concrete used had the design strength of 27 MPa; the actual strength was observed to increase to the compressive strength of 28 MPa at 28 days. Figure 8 demonstrates the prefabrication of experimental specimens, including cage assemblies for re-bars and steel sections and concrete cast followed by Fabrication of the foundation. Figure 8(d) shows specimens prepared to be loaded, including the test setup for actuators and the data acquisition system with gauges.

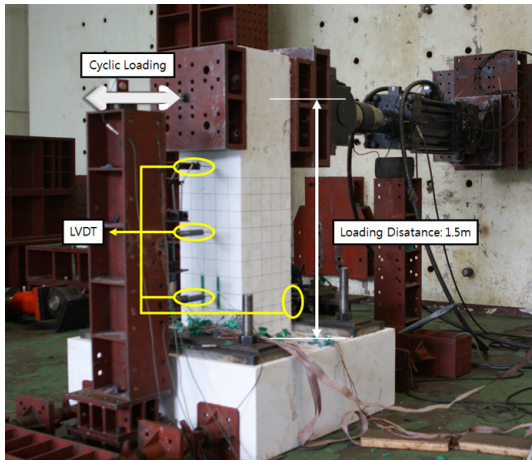


Fig. 4(a). Test setup for the specimens

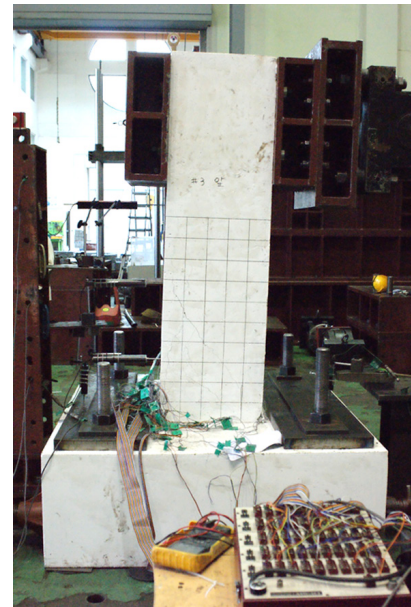


Fig. 6. Deformed specimen under load

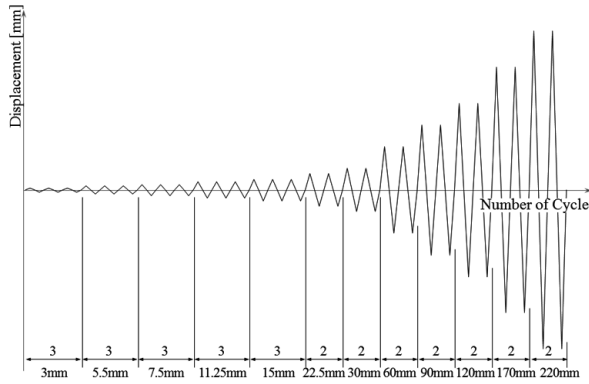


Fig. 4(b). Loading protocol



Fig. 5. Strain gauges of re-bars

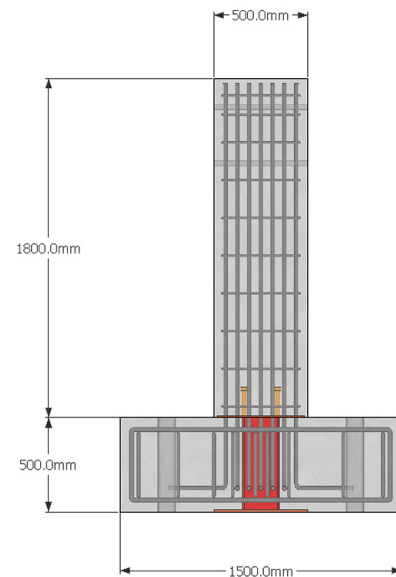


Fig. 7(a). Front view

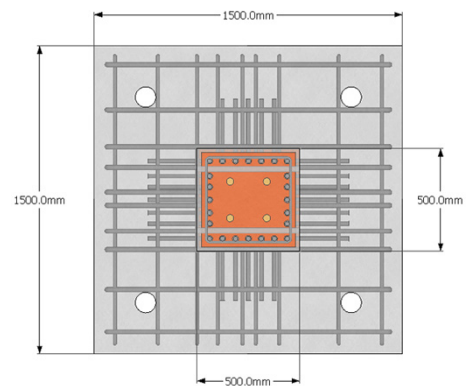


Fig. 7(b). Top view

Fig. 7. Columns and foundations of the specimens



Fig. 8(a). Assembly for re-bars and steel sections



Fig. 8(b). Concrete cast



Fig. 8(c). Fabrication of foundation



Fig. 8(d). Test setup

Fig. 8. Specimen fabrication

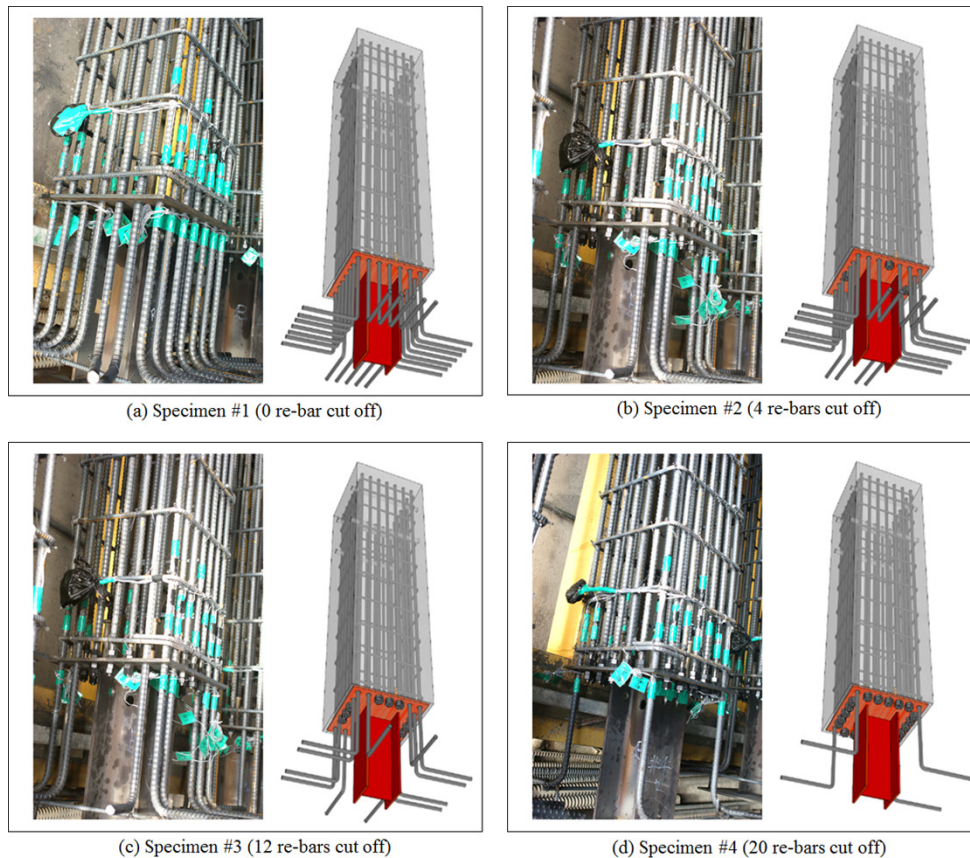


Fig. 9. Specimens #1–4

## 2.2. Preparation of test specimens

Figure 9 illustrates four specimens tested to verify load transfer from re-bars to steel plates above the joints and from the steel plates to re-bars below the joints. The flexural load-bearing capacity of a column with 24 vertical re-bars was compared to that of columns with discontinuous re-bars at joints. The number of discontinuous re-bars at joints used in the column specimens was 0 (0.0%, Specimen #1), 4 (16.7%, Specimen #2), 12 (50.0%, Specimen #3), and 20 (83.3%, Specimen #4), as depicted in Figure 9. Table 1 lists the material properties of the specimens

## 3. Experimental investigation

Figures 10, 11, 12 and 13 demonstrate the hysteretic load–displacement relationships of Specimens #1, #2, #3, and #4, respectively. The displacements were related with strains by means of gauge readings plotted on the load–displacement curves. These displacements were also

related to the analytical data calculated based on strain compatibility, as shown in Figure 13. The comparison between analytical and experimental load–displacement relationship in Figure 13 indicated that the discontinuous 20 re-bars contributed to the moment-resisting capacity. Each specimen demonstrated good ductility and showed a well-established load path. Table 2 presents the measured maximum load resisting capacity of each specimen; as shown in the table, the maximum load resisting capacity decreased as the number of discontinuous reinforcing bars at the joint was increased. Specimen #1, the control specimen with no rebar discontinuities, was compared with the other three specimens to observe their reduction of moment resisting capacity. Moment resisting capacity was reduced by 6% for Specimen #2 with 4 rebar discontinuities, and was reduced by 54.1% for Specimen #4, which lost 20 re-bars at the column joint.

## 4. Analytical results

Analytical investigations indicated by blue dots in Figures 10 through 13 were the flexural load resisting capacity of the specimens with only the remaining re-bars, without considering loads transferred through the two plates above and below the steel section and the steel section at the joint. Figures 10 through 13, which com-

Table 1. Specimen material properties

Material property	
Concrete compressive strength ( $f'_c$ )	27 MPa
Rebar yield strength ( $f_y$ )	400 MPa
Steel yield strength ( $F_y$ )	325 MPa

Table 2. Loadings at maximum load limit state and at the end of testing

Specimen	No. of discontinuous Re-bars	Displacement [mm]		Loading [kN]		
		maximum load limit state	End of test	Maximum load limit state (positive dir.)	Maximum load limit state (negative dir.)	End of test
#1	0	37	60	431.2	-418.5	204.4
#2	4	30	53	399.4	-426.7	201.3
#3	12	45	90	371.4	-383.3	167.9
#4	20	22	60	198.6	-182.4	111.1

pare these analytical investigations with experimental data at the maximum load limit state, elucidate the net flexural load resisting capacity of the specimens which were vertically transferred through the upper plate, the steel section at the joint, and the lower plate. The load–strain relationships of re-bar gauges were converted to a displacement scale by comparing load–strain relationships to the LVDT data which was measured in terms of

displacement. Load–displacement relationships of re-bar gauges were found similar to the load–displacement relationships of LVDTs, as shown in Figures 10 through 13, allowing comparison between strains and displacements. It was possible, then, to compare the analytical data from strain compatibility analysis obtained in terms of strains to LVDT displacement data. Eqn (1) was derived based on strain compatibility to calculate the neutral axis and

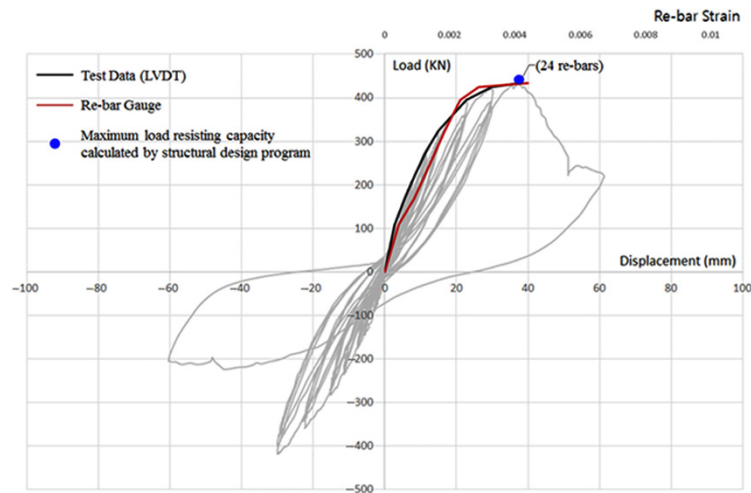


Fig. 10. Load–displacement curve of Specimen #1

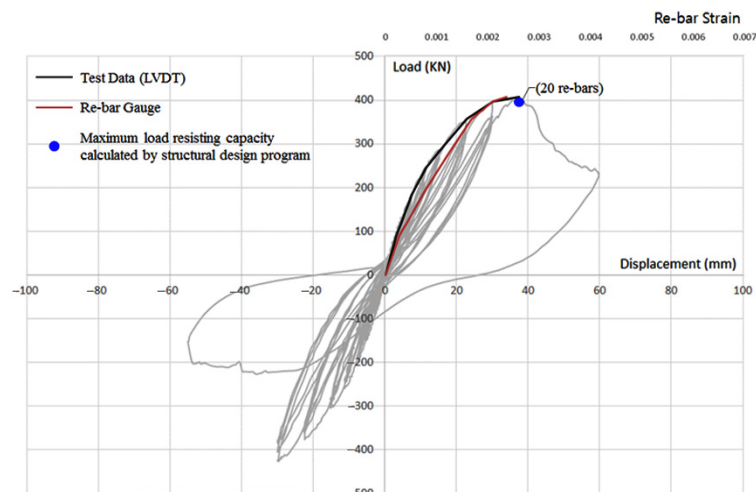


Fig. 11. Load–displacement curve of Specimen #2

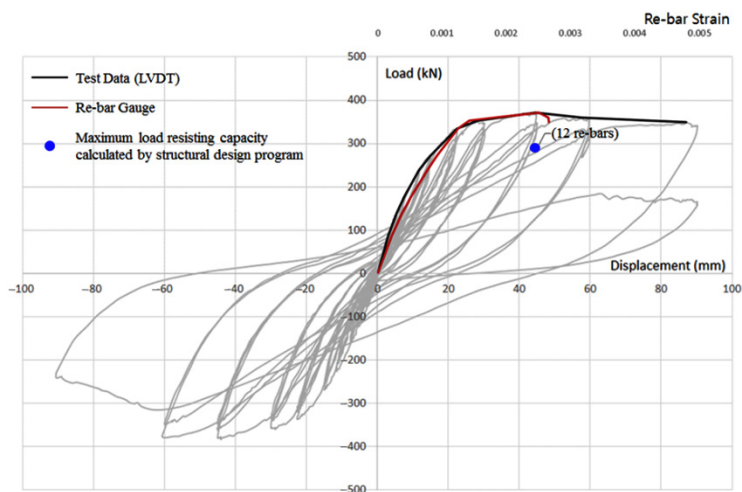


Fig. 12. Load–displacement curve of Specimen #3

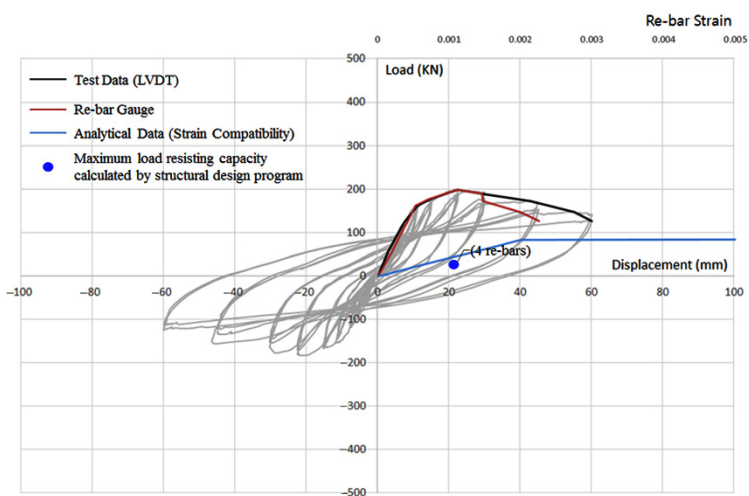


Fig. 13(a). Load–displacement curve of Specimen #4 (unconfined)

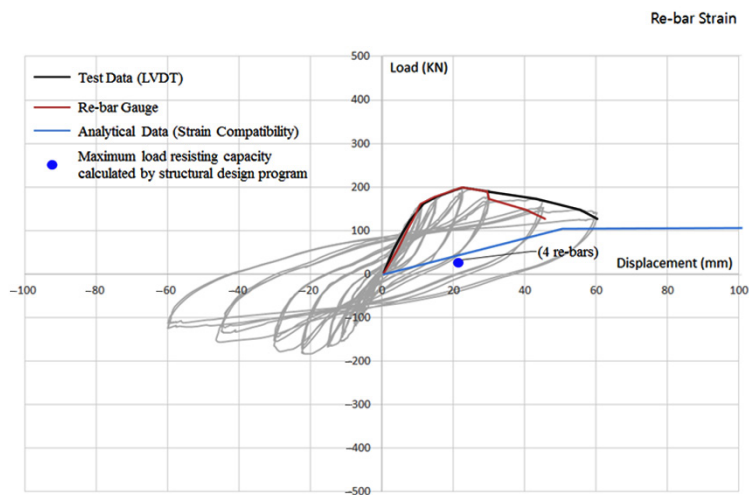


Fig. 13(b). Load–displacement curve of Specimen #4 (confined)

Fig. 13. Load–displacement curve of Specimen #4

nominal moment capacity of the Specimen #4 was calculated by Eqn (2):

$$\alpha f'_c b c + A'_s E_s \frac{\epsilon_c}{c} (c - d'') + \frac{1}{2} b_f E_s \frac{\epsilon_c}{c} (c - d'')^2 =$$

$$A_s f_y + A_f F_y + \frac{1}{2} b_f E_s \frac{\epsilon_c}{c} \{t_f' - (c - d''')\}^2 + A_{wp} F_y +$$

$$A_{wny} E_s \frac{\epsilon_c}{c} \{t_f' - (c - d''')\} +$$

$$\frac{1}{2} A_{wny} E_s \frac{\epsilon_c}{c} \left\{ \left( \frac{\epsilon_{sy}}{\epsilon_c} + 1 \right) c - t_f' - d''' \delta \right\}; \quad (1)$$

$$M_n = \alpha f'_c b c (c - \gamma c) + A'_s E_s \frac{\epsilon_c}{c} (c - d'')^2 +$$

$$\frac{1}{3} b_f E_s \frac{\epsilon_c}{c} (c - d'')^3 + \frac{1}{3} b_f E_s \frac{\epsilon_c}{c} \{t_f' - (c - d''')\}^2 +$$

$$A_s F_y (d - c) + A_f F_y \left( d - c - d' - \frac{t_f'}{2} \right) +$$

$$\frac{1}{2} A_{wp} E_s \frac{\epsilon_c}{c} \{t_f' - (c - d''')\} \left\{ \frac{\epsilon_{sy}}{\epsilon_c} c + (d''' + t_f' - c) \right\} +$$

$$\frac{1}{2} A_{wny} \frac{\epsilon_c}{c} \{t_f' - (c - d''')\} \left[ (d''' + t_f' - c) + \frac{2}{3} \left\{ \frac{\epsilon_{sy}}{\epsilon_c} c + (d''' + t_f' - c) \right\} \right]. \quad (2)$$

Regarding displacement, Figures 13(a) and 13(b) compare the load–displacement curve of Specimen #4 obtained during the test to analytical data from strain compatibility analysis based on unconfined and confined constitutive relationships of concrete.

### 5. Results and comparison of four specimens

The differences were interpreted to arise from the net flexural load resisting capacity of the specimens which were vertically transferred through plates and the steel section at the joints with discontinuous re-bars at joints.

The capacity drop for Specimen #3, with 50% re-bar discontinuities, was found to be only 13.7% relative to the control specimen, indicating that load transfer was relatively well established between the upper rebar, upper plate, steel section at the joint, lower plate, and lower rebar, as shown Figure 3(b). Table 2 lists loadings for each specimen at the maximum load limit state and at the end of testing. The red and blue columns in Figure 14 represent the experimental and analytical flexural capacity (Mn) of the specimens at maximum load limit state, respectively. The discontinued re-bars were omitted in the analytical calculation. The red line with square marks represents the tensile strain of the steel flange at the maximum load limit state. In Figures 15(a) and (b), the blue and purple lines with x marks depict the tensile strain of continuous and discontinued re-bars at the maximum load limit state, respectively. Specimens 2, 3, and 4 showed that the strains in the re-bars and steel flange decreased as more re-bars were cut, as shown in Figures 16(a) and (b). Shortened Discontinued re-bars

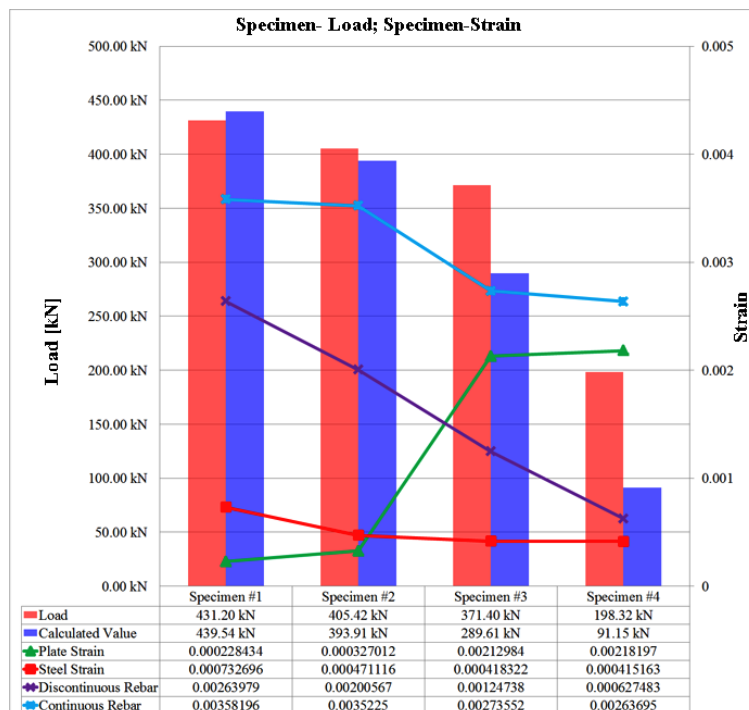
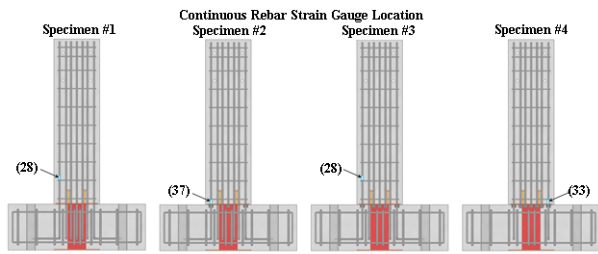
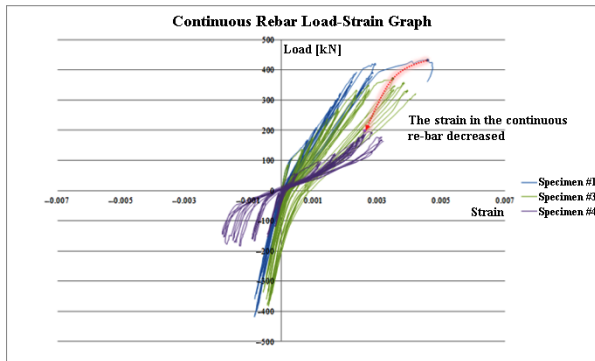


Fig. 14. Influence of discontinued re-bars on the transfer of stresses

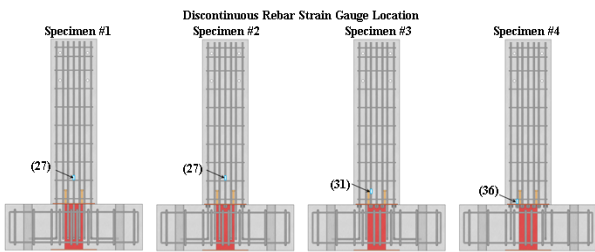


(a) Gauge location of continuous re-bars

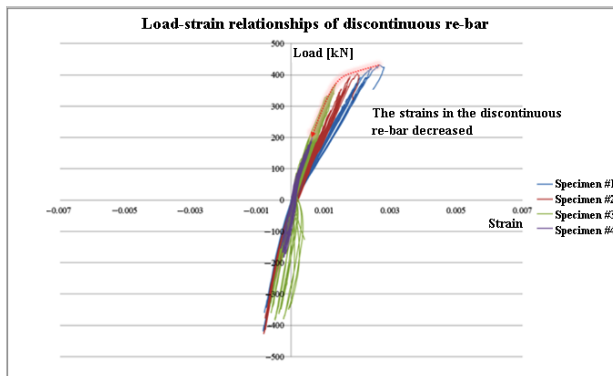


(b) Load-strain relationships of continuous re-bars

Fig. 15. Comparison of test results for four specimens (Continuous re-bars)



(a) Gauge location of discontinuous re-bars



(b) Load-strain relationships of discontinuous re-bars

Fig. 16. Comparison of test results for four specimens (Discontinuous re-bars)

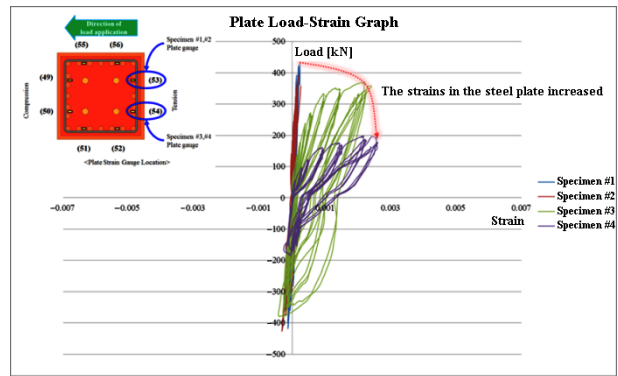


Fig. 17. Gauge location and load-strain relationships of steel plate

decreased the flexural capacity of the specimens at the maximum load limit state by reducing the strains in steel section and all of the re-bars.

However, strain increased in the steel plate as more re-bars were cut, as shown in Specimens 2, 3, and 4, because some of the stress from the discontinued re-bars was transmitted to the steel column through the plate, exhibiting that some portion of the stress from the discontinued re-bars was transferred through the nuts to the steel plate, steel section, plate below and finally to the re-bars below, indicating that not all the stress was resolved. Figure 14 also shows that the experimental values were greater than the analytical calculations in which the stress of discontinued re-bars was neglected, except Specimen 1 where no re-bars were cut. Figures 15 and 16 demonstrate the load-strain relationships of continuous and discontinuous re-bars, respectively, where strain decreased when re-bars were cut. Figure 17 illustrates the load-strain relationships of a steel plate on which the cut re-bars were bolted with nuts. It is noted that the strains in the steel plate increased as re-bars were cut, demonstrated in Specimens 2, 3, and 4. Table 3 summarizes the strains of the selected structural elements of all specimens at the maximum load limit state. Figure 18 illustrates the degradation in flexural moment resisting capacity of columns as rebar discontinuities increased; Table 4 lists the reductions in capacity for each specimen. Figure 19 shows the degrees of deterioration of each specimen, which differed depending on which structural components were damaged. The concrete was most severely damaged in Specimen #1 whereas Specimen #4 showed the least damage on the face of the concrete. As seen in the figure, the concrete deteriorated more as fewer re-bars were discontinued; the least concrete deterioration occurred in Specimen #4 because most structural damage was concentrated on the re-bars with bolt connections, preventing the concrete from suffering severe structural deterioration.

Table 3. Strains of the selected structural elements at the maximum load limit state

Gauge No.		Rebar								
		Compressive				Tensile				
		Specimen #1	Specimen #2	Specimen #3	Specimen #4	Strain	Specimen #1	Specimen #2	Specimen #3	Specimen #4
		Strain				Strain				
11		-0.000557342	-0.000764923	-0.000808525	-0.001230320	27	0.002639790	0.002005670	0.001333880	0.000590517
12		-0.0000612318	-0.000724165	-0.000269192	Gauge malfunction	28	0.002941210	0.002883600	0.002735520	0.000161989
13		-0.001276770	-0.001750700	-0.00138388	-0.001097620	29	0.353362000	0.002810400	0.003843810	0.000722269
14		-0.001252120	-0.000868240	-0.00113459	-0.000238861	30	0.002606610	0.002548800	0.001814200	0.000832221
15		-0.001762070	-0.001754490	-0.00163032	-0.001072980	31	0.003233150	0.003201870	0.001247380	Gauge malfunction
16		-0.002143110	-0.000448338	-0.00159525	-0.001268240	32	0.003304240	Gauge malfunction	0.003617980	0.000742274
17		-0.001531740	-0.000390518	-0.00165212	-0.000399997	33	0.003581960	0.002320360	0.003062540	0.002636950
18		-0.001668230	-0.000136492	-0.00183127	-0.000506157	34	Gauge malfunction	0.003075810	0.003151630	0.000590517
19		-0.001861600	-0.001747850	-0.0025232	-0.001435060	35	0.003410400	0.001653070	0.001360180	0.000594308
						36	0.004250200	0.003470120	0.004166790	0.000627483
						37	0.002955430	0.003522250	0.004128880	0.002508040
Average		-0.001407256	-0.000953968	-0.001425372	-0.000906154	Average	0.030199969	0.002749195	0.002769345	0.001000657
20		-0.001784820	-0.001247380	-0.00100852	Gauge malfunction	38	0.003036000	0.003159640	0.002950690	Gauge malfunction
21		-0.001627480	-0.001375340	-0.00103885	Gauge not installed	39	0.003858740	0.000425589	0.003672010	Gauge not installed
22		-0.000732696	-0.001311640	Gauge not installed	Gauge not installed	40	0.003186710	0.003284330	Gauge not installed	Gauge not installed
23		-0.000700469	Gauge not installed	Gauge not installed	Gauge not installed	41	0.003229360	Gauge not installed	Gauge not installed	Gauge not installed
24		-0.000856865	-0.001347860	Gauge not installed	Gauge not installed	42	0.003273910	0.000981035	Gauge not installed	Gauge not installed
25		-0.000439807	-0.001433160	-0.00085497	Gauge not installed	43	0.002712780	0.003614190	0.002811350	Gauge not installed
26		-0.001925100	-0.001590510	-0.00137819	-0.000928903	44	0.002801870	0.004475790	0.002811350	Gauge malfunction
Average		-0.001152462	-0.001384315	-0.001070133	-0.000928903	Average	0.003157053	0.002656762	0.003061350	-

Continuous Rebar  
Discontinuous Rebar

Continued Table 3

Plate													
Gauge No.	Compressive				Strain	Tensile				Specimen #4	Specimen #3	Specimen #2	Specimen #1
	Specimen #1	Specimen #2	Specimen #3	Specimen #4		Specimen #1	Specimen #2	Specimen #3	Specimen #4				
	Strain					Strain							
49	-0.000070142	-0.000513740	-0.000454973	-0.000147866	52	0.000032227	0.000047393	Gauge malfunction	0.000266349				
50	-0.000469191	0.000269192	Gauge malfunction	-0.000221799	53	0.000228434	0.000327012	0.001378190	0.000187771				
51	-0.000050237	-0.000117535	Gauge malfunction	Gauge malfunction	54	0.000152605	0.000134596	0.002129840	0.002181970				
55	-0.000080568	-0.000177250	-0.000048341	-0.000878666	56	0.000086255	0.000187676	Gauge malfunction	Gauge malfunction				
Average	-0.000167534	-0.000134833	-0.000251657	-0.000416110	Average	0.000124880	0.000174169	0.001754015	0.000878697				
Steel													
Gauge No.	Compressive				Strain	Tensile				Specimen #4	Specimen #3	Specimen #2	Specimen #1
	Specimen #1	Specimen #2	Specimen #3	Specimen #4		Specimen #1	Specimen #2	Specimen #3	Specimen #4				
	Strain					Strain							
1	-0.000299524	-0.000329855	Gauge malfunction	-0.000236965	4	0.000898571	0.000327012	0.00090805	0.000173458				
2	-0.000328907	-0.000446442	-0.000298576	-0.000236965	5	0.000566820	0.000619900	0.000145023	0.000333647				
3	-0.000316585	-0.000404736	Gauge malfunction	-0.000236965	6	Gauge malfunction	0.000466437	0.000201894	0.000496679				
Average	-0.000315005	-0.000393678	-0.000298576	-0.000236965	Average	0.000732696	0.000471116	0.000418322	0.000334595				

Table 4. Number of discontinuous re-bars and moment resisting capacities of each specimen

	Specimen #1	Specimen #2	Specimen #3	Specimen #4
Discontinuous rebar ratio (Number of discontinuous re-bars)	0.0% (0)	16.7% (4)	50.0% (12)	83.3% (20)
Reduction ratio (Moment resisting capacity)	0.0% (646.80 kN-m)	6.0% (608.13 kN-m)	13.7% (557.10 kN-m)	54.0% (297.48 kN-m)

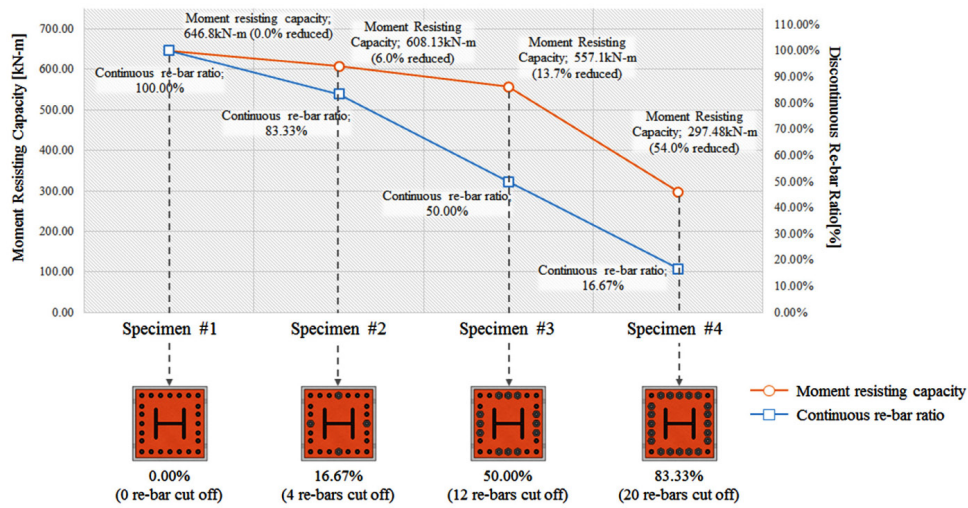


Fig. 18. Maximum moment resisting capacity versus number of continuous reinforcing bars

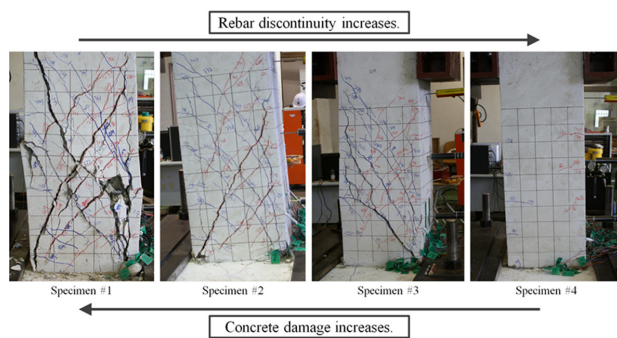


Fig. 19. Degree of deterioration for each specimen versus number of discontinuous reinforcing bars

**Conclusions**

In a previously proposed design for steel beam–column connections for precast concrete frames, there were some spatial conflicts in structural details between vertical column re-bars and column brackets. This paper investigated the solution of disconnecting vertical re-bars to make the structural details constructible. Re-bars connected to steel plates by bolts above and below column steel are discontinued at the joint to provide space for connections between column brackets and beam steels. This strategy provided space for connections at beam–column joints for steel–concrete composite frames, with the trade-off of some reductions in moment resisting capacity. However, this reduction in strength could be minimized or counterbalanced by introducing high-strength steel plate at the joints. In experimental specimens employing this strat-

egy, the loading path was found to be well established, allowing load transfer between the upper rebar, upper plate, steel section at the joint, lower plate, and lower re-bar. Experimental investigations demonstrated that the load resisting capacities decreased only somewhat when a few re-bars were disconnected, but deteriorated more rapidly as additional re-bars were removed: a reduction of only 6% in load resisting capacity was observed for the specimen with 17% discontinuous re-bars, whereas a 54% strength reduction was found for the specimen with 83% discontinuous re-bars. Experiments showed how loads from vertical steel reinforcements that were cut off at the joints were transferred to the steel plate. The test results also demonstrated that the flexural capacities were reduced in specimens with discontinuous vertical re-bars: reductions of 6.0%, 13.7%, and 54.0% were observed for columns with 4 (16.7%), 12 (50.0%), and 20 (83.3%) discontinuous vertical re-bars, respectively. The test results can be used to design vertical reinforcing bars and column joints that can provide space for column brackets to which steel members of beams are connected. The findings in this paper are expected to provide valuable data for research on replacing conventional beam–column joints by extended beam end-plates.

**Acknowledgements**

This research was supported by Basic Science Research Program through the National Research Foundation of Korea(NRF) funded by the Ministry of Education (No. 2009-0090554), and also by the Ministry of Land,

Infrastructure and Transport (MOLIT) of the Korean government and the Korea Agency for Infrastructure Technology Advancement (KAIA) (No. 14AUDP-B068892-02).

## References

- Ataei, A.; Bradford, M. A.; Valipour, H. R. 2015. Experimental study of flush end plate beam-to-CFST column composite joints with deconstructed bolted shear connectors, *Engineering Structures* 99: 616–630. <https://doi.org/10.1016/j.engstruct.2015.05.012>
- Bjorhovde, R.; Colson, A.; Brozzetti, J. 1990. Classification system for beam-to-column connections, *Journal of Structural Engineering* 116(11): 3059–3076. [https://doi.org/10.1061/\(ASCE\)0733-9445\(1990\)116:11\(3059\)](https://doi.org/10.1061/(ASCE)0733-9445(1990)116:11(3059))
- Deierlein, G. G.; Sheikh, T. M.; Yura, J. A.; Jirsa, J. O. 1989. Beam-column moment connections for composite frames: Part 2, *Journal of Structural Engineering* 115(11): 2877–2896. [https://doi.org/10.1061/\(ASCE\)0733-9445\(1989\)115:11\(2877\)](https://doi.org/10.1061/(ASCE)0733-9445(1989)115:11(2877))
- Fang, L. X.; Chan, S. L.; Wong, Y. L. 1999. Strength analysis of semi-rigid steel-concrete composite frames, *Journal of Constructional Steel Research* 52(3): 269–291. [https://doi.org/10.1016/S0143-974X\(99\)00032-2](https://doi.org/10.1016/S0143-974X(99)00032-2)
- Hajjar, J. F. 2002. Composite steel and concrete structural systems for seismic engineering, *Journal of Constructional Steel Research* 58(5): 703–723. [https://doi.org/10.1016/S0143-974X\(01\)00093-1](https://doi.org/10.1016/S0143-974X(01)00093-1)
- Hong, W. K.; Park, S. C.; Kim, J. M.; Lee, S. G.; Kim, S. I.; Yoon, K. J.; Lee, H. C. 2008a. Composite beam composed of steel and precast concrete (Modulized Hybrid System, MHS). Part I: Experimental investigation, *The Structural Design of Tall and Special Buildings* 19: 275–289.
- Hong, W. K.; Kim, J. M.; Park, S. C.; Kim, S. I.; Lee, S. G.; Lee, H. C.; Yoon, K. J. 2008b. Composite beam composed of steel and precast concrete (Modulized Hybrid System, MHS). Part II: Analytical investigation, *The Structural Design of Tall and Special Buildings* 18: 891–905. <https://doi.org/10.1002/tal.484>
- Hong, W. K.; Lee, Y. J.; Kim, S. K.; Kim, S. I.; Yun Y. J. 2015. Analytical investigation of hybrid composite precast beams with modified strain compatibility for entire history of nominal flexural capacity, *The Structural Design of Tall and Special Buildings* 24: 835–852. <https://doi.org/10.1002/tal.1214>
- Hu, F.; Shi, G.; Bai, Y.; Shi, Y. 2014. Seismic performance of prefabricated steel beam-to-column connections, *Journal of Constructional Steel Research* 102: 204–216. <https://doi.org/10.1016/j.jcsr.2014.07.012>
- Kataoka, M. N.; El Debs, A. L. H. 2014. Parametric study of composite beam-column connections using 3D finite element modelling, *Journal of Constructional Steel Research* 102: 136–149. <https://doi.org/10.1016/j.jcsr.2014.07.006>
- Kumar, S. R. S.; Smitha, M. S. 2013. Steel–concrete composite flange plate connections: Cyclic performance and tests, *Journal of Constructional Steel Research* 82: 216–222. <https://doi.org/10.1016/j.jcsr.2013.01.003>
- Liew, J. Y. R.; Teo, T. H.; Shanmugam, N. E. 2004. Composite joints subject to reversal of loading –Part 1: experimental study, *Journal of Constructional Steel Research* 60(2): 221–246. <https://doi.org/10.1016/j.jcsr.2003.08.010>
- Liew, J. Y. R.; Teo, T. H.; Shanmugam, N. E.; Yu, C. H. 2000. Testing of steel–concrete composite connections and appraisal of results, *Journal of Constructional Steel Research* 56(2): 117–150. [https://doi.org/10.1016/S0143-974X\(99\)00099-1](https://doi.org/10.1016/S0143-974X(99)00099-1)
- Qin, Y.; Chen, Z.; Wang, X. 2014a. Experimental investigation of new internal-diaphragm connections to CFT columns under cyclic loading, *Journal of Constructional Steel Research* 98: 35–44. <https://doi.org/10.1016/j.jcsr.2014.02.014>
- Qin, Y.; Chen, Z.; Wang, X. 2014b. Elastoplastic behavior of through-diaphragm connections to concrete-filled rectangular steel tubular columns, *Journal of Constructional Steel Research* 93: 88–96. <https://doi.org/10.1016/j.jcsr.2013.10.011>
- Qin, Y.; Chen, Z.; Rong, B. 2014c. Component-based mechanical models for axially-loaded through-diaphragm connections to concrete-filled RHS columns, *Journal of Constructional Steel Research* 102: 150–163. <https://doi.org/10.1016/j.jcsr.2014.06.016>
- Salvatore, W.; Bursi, O. S.; Lucchesi, D. 2005. Design, testing and analysis of high ductile partial-strength steel–concrete composite beam-to-column joints, *Computers & Structures* 83(28): 2334–2352. <https://doi.org/10.1016/j.compstruc.2005.03.028>
- Sheikh, T. M.; Deierlein, G. G.; Yura, J. A.; Jirsa, J. O. 1989. Beam-column moment connections for composite frames: Part 1, *Journal of Structural Engineering* 115(11): 2858–2876. [https://doi.org/10.1061/\(ASCE\)0733-9445\(1989\)115:11\(2858\)](https://doi.org/10.1061/(ASCE)0733-9445(1989)115:11(2858))
- Simões Da Silva, L.; Simões, R. D.; Cruz, P. J. S. 2001. Experimental behaviour of end-plate beam-to-column composite joints under monotonical loading, *Engineering Structures* 23(11): 1383–1409. [https://doi.org/10.1016/S0141-0296\(01\)00054-2](https://doi.org/10.1016/S0141-0296(01)00054-2)
- Zhang, Y. F.; Zhao, J. H.; Cai, C. S. 2012. Seismic behavior of ring beam joints between concrete-filled twin steel tubes columns and reinforced concrete beams, *Engineering Structures* 39: 1–10. <https://doi.org/10.1016/j.engstruct.2012.01.014>

**Ju-Yun HU.** She is currently enrolled as a Master candidate in the Department of Architectural Engineering at Kyung Hee University, Republic of Korea. Her research interest includes precast composites structures and development of construction method with structural efficiency. Miss Ju-Yun Hu performed extensive finite element analysis using Abaqus to investigated precast steel concrete composite frames.

**Won-Ke HONG.** Dr. is a professor of Architectural Engineering at Kyung Hee University. Dr. Hong received his masters and PhD degrees from UCLA, and he worked for Englel Kirk and Hart, Inc. (USA), Nihon Sekkei (Japan) and Samsung Engineering and Construction Company (Korea) before he joined Kyung Hee University (Korea). He also has professional engineering license from both Korea and USA. Dr Hong has more than 30 years of professional experience in structural engineering. His research interests include a new approach to construction technologies based on value engineering with hybrid composite structures. He provided many useful solutions to the current structural design and construction technologies issues as a result of his research that combines structural engineering with construction technologies. He is the author of numerous papers and patents both in Korea and USA. Currently, Dr Hong is developing new connections that can be used with various types of frames including hybrid steel–concrete precast composite frame (SMART frame), precast frame and steel frame. These connections would contribute to the modular construction of heavy plant structures and buildings as well.